Understanding chemical ordering in intermetallic clathrates from atomic scale simulations

Mattias Ångqvist and Paul Erhart*

Chalmers University of Technology, Department of Physics, S-412 96 Gothenburg, Sweden

E-mail: erhart@chalmers.se

Abstract

Intermetallic clathrates exhibit great variability with respect to elemental composition and distribution. While this provides a lot of flexibility for tuning properties it also poses a challenge with regard to developing a comprehensive understanding of these systems. Here, we employ a combination of alloy cluster expansions and density functional theory calculations to exhaustively sample the compositional space with *ab-initio* accuracy. We apply this methodology to study chemical ordering and related properties in the clathrate systems $Ba_8Al_xSi_{46-x}$, $Ba_8Al_xGe_{46-x}$, $Ba_8Ga_xGe_{46-x}$, and $Ba_8Ga_xSi_{46-x}$ as a function of composition and temperature. We achieve very good agreement with the available experimental data for the site occupancy factors (SOFs) even for stoichiometries outside the composition range considered during construction of the cluster expansions. This validation enables us to reconcile the variations in the experimental data and explain non-monotonic variations of the SOFs. In particular, we provide a rationale for the extreme SOF behavior with varying composition observed in Al based clathrates. Furthermore, we quantify the effect of chemical ordering on both heat capacity and lattice expansion. Finally, we determine the effect of chemical

*To whom correspondence should be addressed

disorder on the displacements of the guest species (Ba), which enables us to at least partially explain experimental observations of the nuclear density of Ba in different clathrates.

Introduction

Clathrates represent a broad class of chemical substances with a defined lattice structure that can trap atomic or molecular species.[1] In particular, so-called intermetallic clathrates such as $Ba_8Ga_{16}Ge_{30}$ or $Sr_8Ga_{16}Ge_{30}$ have received a lot of attention due to their thermoelectric performance.[2–6] In these systems alkaline and earth alkaline but also some rare earth atoms can occupy cages in the host structure, which is most commonly composed of elements from groups 13 and 14 although other constituents are possible.[7] These structures are realizations of the Zintl concept, i.e. the stoichiometric compounds are fully charge balanced, small gap semiconductors.[2,7–9] In practice, deviations from perfect stoichiometry are common leading to intrinsically doped materials, a feature that can be beneficial, for example for manipulating electrical transport properties.

Clathrates are classified according to their symmetry.[2,7] The majority of known intermetallic clathrates belong to type I and crystallize in space group $Pm\bar{3}n$ (international tables of crystallography number 223).[7] Many of the compounds studied so far have the general composition $A_8B_{16}C_{30}$, where B and C form the host structure and occupy $6c$, $16i$, and $24k$ Wyckoff sites (Fig. 1).[9] While it is most common for the guest species A to be cationic and B and C to be anions, there also exist so-called inverse (cationic) clahtrates, in which the host-guest polarity is reversed.[10]

Experimental measurements of the site occupancy factors (SOFs) in many clathrates show that the elemental distribution over the different crystallographic sites is not simply random.[3] For example in the case of $Ba_8Ga_{16}Ge_{30}$, analysis of diffraction data yields Ga occupancies between 60 and 76% for the $6c$ site, which deviates considerably from the value of 35% corresponding to the stoichiometry of the compound.[11] The experimental observations

have been condensed into a set of rules for the SOFs,[3] partially based on calculations,[12] which have shown that bonds between trivalent species are energetically unfavorable.

The degree of chemical order has been found to vary not only between different compounds but also with stoichiometry with subsequent effects on the host atom structure.[3,13,14] By extension, chemical order has also been shown to impact the transport properties in these materials.[15] This suggests that a fine control of properties, in particular pertaining to transport, can be achieved by adjusting composition and stoichiometry. As a result of the complexity of navigating this multidimensional space as well as the experimental effort required to resolve order in the form of SOFs, this is, however, a very challenging task.[16]

Here, we therefore present a systematic computational study of chemical order and its effect on structure and thermodynamics in a series of ternary intermetallic clathrates with A=Ba, B=Al/Ga, and C=Si/Ge. To this end, we employ a combination of first-principles calculations and lattice Hamiltonians (alloy cluster expansions) that enables us to sample both temperature and composition space with high accuracy. Where comparison is possible our simulations closely match experimental data, which allows us to reveal the general behavior of these materials and effects that are not immediately apparent from the experimental data. We demonstrate that by varying the composition of these materials the SOFs and thus the degree of chemical ordering can be altered dramatically. Furthermore the chemical ordering is shown to systematically affect the average displacement of the guest species (Ba). This provides a key to understanding the origin of the non-spherical nuclear density of Ba observed experimentally in some clathrates.[13]

Recent computational work on inorganic clathrates has addressed ground state structures in $Ba_8Ga_{16}Ge_{30}$ (Ref. 15) as well as $Ba_8Al_xSi_{46-x}$ (Ref. 17) with an emphasis on electronic properties. In addition, the SOFs in stoichiometric $Ba_8Ga_{16}Ge_{30}$ have been analyzed.[15] In the present work, we go beyond these studies by addressing the variation of the SOFs with composition and temperature, and by conducting this investigation for a series of clathrates. Furthermore, we emphasize the coupling between order and thermodynamic properties, as

well as the connection to experiment.

The remainder of this paper is organized as follows. In the next section, we outline the construction of the alloy cluster expansions used in this work as well as the density functional theory calculations that were carried out to obtain input data. This is followed by the presentation of results for stoichiometric materials, in particular the temperature dependence of the site occupancy factors, which sets up an analysis of the contributions of chemical order on heat capacity and lattice expansion. We then extend the scope to non-stoichiometric compositions, which provides a comprehensive picture of ordering in these materials, along with a rather extensive comparison with experimental data. Finally, we describe the coupling between chemical order and the off-center displacement of the guest species (Ba) atoms.

Methodology

Alloy cluster expansions

Given a 16:30 ratio between group 13 and 14 elements, there are $46!/30!/16! \approx 10^{12}$ different ways of distributing the atoms in the primitive unit cell. While this number is reduced by about one orders of magnitude when taking into account symmetry, the remaining space is still extremely large and cannot be sufficiently sampled by density functional theory (DFT) calculations alone. Here, we therefore resort to the alloy cluster expansion (CE) technique which allows at least in principle an exact mapping of ordering energetics onto an effective lattice Hamiltonian.[18,19] The energy of the system is expressed in the form of a generalized Ising model, which not only includes pair (second order) terms but also higher order "clusters" including e.g., triplets (involving three sites) or quadruplets (four sites). Using a CE

the energy can be formally written as

$$E(\boldsymbol{\sigma}) = E_0 + \sum_{\alpha} m_\alpha J_\alpha \bar{\Pi}_\alpha(\boldsymbol{\sigma}). \tag{1}$$

Here, J_α are the so-called effective cluster interactions (ECIs) that are associated with the symmetry inequivalent clusters α, which occur with multiplicity m_α. The occupation of different sites is represented by the "spin" vector $\boldsymbol{\sigma}$, each value of which indicates the occupation of a site in the system (here, -1 and $+1$ for group-13 and 14 elements, respectively). Finally, $\bar{\Pi}_\alpha$ is a symmetrized product over the spin variables, which, approximately speaking, represents the average occupation ("decoration") of cluster α by the species considered in the CE. It is important to emphasize that while the CE is itself restricted to a rigid lattice, atomic relaxation and strain contributions to the energy are effectively incorporated in the ECIs if the CE is trained using relaxed structures. Furthermore, we note that the expansion Eq. (1) is not restricted to the energy but can be extended to other properties including, e.g., electronic properties[15] or, as in the present work, the lattice parameter.

In order to construct the CE, i.e. obtain the set of ECIs representing the energy landscape for a certain material, we employed compressive sampling[20] in conjunction with the split-Bregman algorithm,[21,22] which has been shown to be very efficient for constructing physically sound and very accurate CEs.[23] To this end, we used our in-house integrated cluster expansion toolkit (ICET). Recently, we successfully employed the same approach to describe chemical ordering and its effect on transport properties in stoichiometric $Ba_8Ga_{16}Ge_{30}$.[15]

For each of the four elemental combinations, we constructed a CE based on a set of 290 structures for $Ba_8Ga_xGe_{46-x}$ and 240 for the remaining three alloys, which were relaxed and characterized using DFT calculations. For $Ba_8Ga_xGe_{46-x}$ the set included 101, 163, 21 and 6 structures with stoichiometries of 16:30, 15:31, 14:32 and 13:33, respectively. For the remaining three materials the set comprised 171, 42, 21 and 6 structures with stoichiometries of 16:30, 15:31, 14:32 and 13:33, respectively.

The cluster vector space considered during the optimization of the ECIs included 90 clusters up to third order. The μ parameter, which controls the sparsity of the CS solution, was set to 0.001 while the λ-parameter that enters in the split-Bregman algorithm was set to 100 (see Ref. 23 for a discussion of these parameters). These values were chosen based on a preliminary screening study. This specific choice has, however, only a minor impact on the final results and mostly affects the efficiency of the optimization procedure.

We note that experimentally vacancies are known to be present in notable concentrations, especially for samples that are very far from the stoichiometric composition, e.g., for $Ba_8Ga_xGe_{46-x}$ with $x = 3.5 - 5$.[24] Here, we do not include this effect, whence our results for these extreme compositions should be regarded as idealized approximations of the real behavior.

The CEs were sampled using Monte Carlo (MC) simulations. Simulated annealing runs were carried out by initializing a system composed of one unit cell at 1200 K, after which the temperature was gradually reduced at a rate of at most 25 K/20,000 MC cycles.[25] At each temperature the system was equilibrated for 2,000 MC cycles, followed by 30,000 MC cycles during which statistics were gathered. In addition, simulations were carried out at constant temperature and variable composition using the variance constrained semi-grandcanonical ensemble.[26]

Electronic structure calculations

The parametrization of the CE Hamiltonian described in the previous section requires total energies for a set of representative structures. To this end, density functional theory (DFT) calculations were carried out using the projector augmented wave method[27,28] as implemented in the Vienna ab-initio simulation package.[29,30] The generalized gradient approximation as parametrized in Ref. 31 was employed to represent the exchange-correlation functional. The Brillouin zone was sampled using a Γ-centered $3 \times 3 \times 3$ $\boldsymbol{k}$-point mesh and the plane wave basis set was expanded up to cutoff energies of 319 eV ($Ba_8Al_xSi_{46-x}$,

$Ba_8Ga_xSi_{46-x}$), 312 eV ($Ba_8Al_xGe_{46-x}$), and 243 eV ($Ba_8Ga_xGe_{46-x}$).

Structures comprising a single unit cell of 54 atoms were created by randomly assigning Ga and Ge atoms to the 6*c*, 16*i*, and 24*k* Wyckoff sites of the host structure. For each structure both the ionic positions and the cell metric were fully relaxed until atomic forces were less than 10 meV/Å and absolute stresses below 0.1 kbar.

We note that more refined algorithms are available for generating input structures.[23,32] They are, however, difficult if not prohibitive to apply in the present context due to the very large number of possible chemical distributions that can be realized already for the primitive unit cell. The validation presented below demonstrates though that the approach taken here succeeds in providing predictive as well as accurate CEs.

For the ground state structures obtained by simulated annealing (see below) we evaluated the thermal lattice expansion and heat capacity at the level of the quasi-harmonic approximation using the PHONOPY package.[33] To this end, we conducted additional calculations at several volumes spanning a range of approximately $0.85a_0$ to $1.05a_0$, where a_0 is the calculated lattice parameter.

Results and discussion

Validation of cluster expansions

The performance of each CE was evaluated using the leave-one-out cross-validation score and the final CEs achieved very low scores of 0.6, 0.8, 0.8, 1.2 meV/atom for $Ba_8Ga_xGe_{46-x}$, $Ba_8Al_xGe_{46-x}$, $Ba_8Ga_xSi_{46-x}$and $Ba_8Al_xSi_{46-x}$, respectively. This accuracy is not restricted to stoichiometric compositions but applies to a wide concentration range (Fig. 2).

The ECIs decrease in magnitude by approximately one order of magnitude for each increase in order (Fig. 3). The singlet interactions exhibit a clear hierarchy where $6c > 24k > 16i$, which implies that in the absence of group-13/group-13 interactions the occupation of 6*c* sites is energetically the most favorable.

One can furthermore observe that the pair interactions are considerably larger if the clathrate contains Al compared to Ga. As will be discussed below, this causes an inversion of the ordering of the occupation factors for $24k$ and $16i$ sites in $Ba_8Al_xSi_{46-x}$ and $Ba_8Al_xGe_{46-x}$, compared to the Ga-containing variants. Beyond-nearest-neighbor pair as well as triplet terms are generally much smaller and can be even set to zero without a big loss of accuracy, in agreement with similar observations for $Ba_8Al_xSi_{46-x}$ and $Sr_8Al_xSi_{46-x}$.[17]

The ordering of the singlet ECIs is in line with the established rule that at least for Ga-based clathrates the $16i$ site is preferentially occupied by group-14 species.[12] As will be shown below, this rule *alone* is, however, insufficient to explain the variation of the SOFs in non-stoichiometric Al-based clathrates since pair interactions play an important role.

Using simulated annealing we determined the ground state structures at stoichiometric composition, which were subsequently relaxed at the DFT level. For all four materials, the CEs predicted the DFT energy of the ground state structure to within 2 meV/atom. In all cases, the chemical distribution corresponds to the one reported previously for $Ba_8Ga_{16}Ge_{30}$[15] and the ground state structures belong to space group $R3$ (International Tables of Crystallography no. 146) and are provided in the Supplementary Information.

Stoichiometric compositions

Site occupancy factors

Following the successful validation of the CEs, further MC simulations were carried out in order to gather statistics concerning the elemental distribution and in particular the site occupancy factors (SOFs) as a function of both composition and temperature.

We first consider the behavior of the stoichiometric systems (group-13:group-14 = 16:30). The materials exhibit some qualitative similarities in the temperature dependence of the SOFs (Fig. 4). At high temperatures (1000–1200 K) the SOF for $6c$ sites ranges from 55 to 65% while for $16i$ sites it falls between 20 and 30% and for $24k$ sites values from 30 to 40% are obtained. The statistical limit of 16:30=35% is only reached for all sites in the very high

temperature limit ($> 20000\,\mathrm{K}$).

For all four systems, the SOFs for $6c$ and $24k$ sites approach 50% at low temperatures, whereas the $16i$ SOF converges to 6.25%. Ultimately, this leads to the ground state structure described above.[15] It is interesting to note that the SOFs for this structure coincide with those of the lowest energy structure described in Ref. 12, which was obtained by simultaneously minimizing the $16i$ SOF and the number of Ga–Ga bonds.

While the four materials considered here exhibit very similar behavior in the low and high-temperature limits, there are clear differences in the intermediate temperature region. Most notably, we obtain higher $6c$ SOFs for the Ga-based clathrates, which can be traced back to the ECIs according to which the pair interactions are weaker than in the case of the Al-based clathrates. As a result, the Ga-based clathrates can occupy more of the energetically favorable $6c$ sites tolerating the cost of relatively more Ga-Ga nearest neighbors.

Heat capacity

The variation of chemical order with temperature is driven by the balance between energy and entropy. Hence, there should also be a configurational energy term that contributes to the heat capacity of the material. The latter can be obtained from the temperature dependence of the average energy $\langle E \rangle$ recorded during MC sampling or, more directly, the variance of the energy $\langle \Delta E^2 \rangle$ according to

$$\Delta c^{\mathrm{chem}} = \left\langle \Delta E^2 \right\rangle \Big/ k_B T^2. \tag{2}$$

According to the MC simulations, at the stoichiometric composition, the contribution to the heat capacity due to chemical order can reach values of up to $15\,k_B$/unit cell in the case of $Ba_8Ga_{16}Ge_{30}$ and $Ba_8Al_{16}Si_{30}$ and of about $10\,k_B$/unit cell for $Ba_8Ga_{16}Si_{30}$ and $Ba_8Al_{16}Ge_{30}$ [Fig. 5(a)]. By comparison with the temperature variation of the SOFs (Fig. 4) it is apparent that $\Delta c_v^{\mathrm{chem}}$ becomes maximal approximately in those temperature regions, at which the

SOFs undergo the largest change. This effect is about one order of magnitude smaller than the vibrational contribution to the (isobaric) heat capacity. The latter can be obtained from calculations of the phonon density of states in the quasi-harmonic approximation, which for the ground state structures yields values between 1200 ($Ba_8Al_{16}Si_{30}$) to 1400 J/mol K ($Ba_8Ga_{16}Ge_{30}$) 144 to 168 k_B/unit cell in the temperature range between 300 and 900 K and thus above the Debye temperature, which is commonly around 300 K.

In the experimental literature several studies have reported anomalies in the temperature dependence of the heat capacity of clathrates.[34,35] In particular, May *et al.* observed an abrupt increase in the heat capacity of nearly stoichiometric $Ba_8Ga_{16}Ge_{30}$ at about 650 K by 0.03 J/mol/g=15 k_B/unit cell, which is comparable in magnitude to the contribution of chemical order predicted above [Fig. 5 (a)]. Furthermore, the temperature of 650 K, at which the feature is observed, falls in the temperature range of 600 to 700 K, in which one can expect the chemical order to be frozen in (see below). This suggests that the observed jump in heat capacity could be at least partly caused by chemical ordering. We note that this feature in the heat capacity is not observed in all studies. This could be caused by different heating/cooling rates as well as the sensitivity of Δc^{chem} to composition (see Fig. S3 in the Supplementary Information).

Chemical expansion

From the configurations, for which DFT calculations have been conducted, it is apparent that the degree of chemical order also affects the lattice parameter. To provide a more quantitative description of this coupling, additional CEs for the cell volume were constructed and sampled in parallel during the simulated annealing simulations described above. (Details pertaining to the construction of these CEs can be found in the Supplementary Information).

The results demonstrate that chemical disordering can change the lattice parameter by as much as 0.08 Å over the temperature range from 0 to 1200 K, both in the negative [$Ba_8Ga_{16}Si_{30}$ in Fig. 5(b)] and positive direction [$Ba_8Al_{16}Ge_{30}$, $Ba_8Ga_{16}Ge_{30}$ in Fig. 5(b)].

The effect is only negligible in the case of $Ba_8Al_{16}Si_{30}$. The variation of the lattice parameter with order translates to a chemical contribution α_l^{chem} to the linear thermal expansion coefficient. It is largest in the case of $Ba_8Al_{16}Ge_{30}$ where it reaches 1.6×10^{-6}/K [Fig. 5(b)] to be compared with a thermal expansion coefficient due to phonons obtained in the quasi-harmonic approximation of $\alpha_l^{\mathrm{phonon}} = 17 \times 10^{-6}$/K [Fig. 5(c)]. The chemical expansion in these systems is thus typically at least one order of magnitude smaller than the phononic contribution.

Non-stoichiometric compositions

One can readily synthesize non-stoichiometric intermetallic clathrates with compositions that deviate substantially from the ideal 16:30 ratio between trivalent and tetravalent ions.[3,14] Non-stoichiometry is often desirable since it provides a convenient means for tuning the charge carrier concentration in these small band gap systems by (intrinsic) doping. As will be shown in the following, there is an intimate and non-monotonic coupling between the SOFs and the composition that translates into distinct changes in the structure of the cages (see below).

All four systems were sampled at several different temperatures. In addition, we conducted simulated annealing runs, in which the temperature was reduced to zero Kelvin in order to obtain purely energy optimized "ground state" structures.

Site occupancy factors

For the Ga based clathrate systems the SOFs show a relatively smooth variation with composition. The SOFs increase in the order $16i - 24k - 6c$, which corresponds to the energetic ordering of the singlet ECIs [Fig. 3(a,b)]. At the same time the number of Ga–Ga neighbors decreases continuously with decreasing Ga content [Fig. 6(a,b)]. This observation correlates with Ga–Ga repulsion being weaker than Al–Al repulsion as evident from the pair ECIs (Fig. 3).

A compilation of experimental SOFs from various sources[9,36–39] reveals that the calculated SOFs for $Ba_8Ga_xSi_{46-x}$ are in excellent agreement with these data, and in fact clearly reveal the chemical trends in this material.

In contrast to the Ga based materials, in the case of the Al containing systems we observe a very pronounced, non-monotonic dependence of the SOFs on Al content [Fig. 7(c,d)], which is in very good agreement with available experimental data.[9,13,14,40]

The composition dependence exhibits two distinct regions that meet at $x \approx 14$, which becomes even more apparent in the zero temperature limit (Fig. 8). For $x > 14$, the SOFs follow the same order as in the case of the Ga based clathrates, whereas the $24k$ and $16i$ SOFs are reversed for $x \lesssim 14$. This behavior can be rationalized by invoking not only the singlet ECIs but also the pair interactions (Fig. 3).

First we note that for compositions below $x = 14$ (but not above) it is possible to accommodate all Al atoms on $6c$ and $16i$ sites without the need to occupy $24k$ sites. Since there are no bonds between $16i$ and $6c$ sites (Fig. 1), this strategy effectively avoids nearest neighbor Al–Al pairs. Since the pair ECIs for the Al systems are larger by a factor of two to five compared to the Ga containing clathrates, avoiding Al–Al neighbors is energetically more important and $16i$ sites become effectively favored over $24k$ sites. The strength of the Al–Al repulsion is also apparent in the much lower fraction of Al–Al neighbors, which is below 2% for practically the entire temperature-composition plane [Fig. 6(c,d)].

The effect of the pair ECIs is even notable when comparing $Ba_8Al_xGe_{46-x}$ and $Ba_8Al_xSi_{46-x}$, as in the latter case the peak in the $16i$ SOF around $x = 14$ is less pronounced [Fig. 7(c,d)], which is in line with the lower pair ECIs of $Ba_8Al_xSi_{46-x}$ [Fig. 3(c,d)].

Similar features as the ones described above were already observed in the experimental data for both $Ba_8Al_xSi_{46-x}$ and $Ba_8Al_xGe_{46-x}$, which prompted the formulation of a set of rules for the SOFs.[3] The present analysis provides a rigorous basis for these rules and demonstrates how the underlying interaction strengths can be obtained quantitatively, which allows one to extend the approach more easily to a larger class of clathrates. We note that

the variation of the SOFs at zero temperature described here (Fig. 8) was also observed in a recent simulation study that focused on the ground state structures in $Ba_8Al_xSi_{46-x}$ and $Sr_8Al_xSi_{46-x}$.[17]

The temperature dependence of the SOFs predicted by our simulations represents the behavior of materials that have achieved thermodynamic equilibrium with regard to the distribution of different chemical species over the available lattice sites. Experimentally, equilibrium can be expected to be achieved only above a certain minimum temperature, corresponding to the onset of mobility for intrinsic defects that can mediate atomic rearrangement.[41] This temperature range can thus be estimated by comparison of calculated and experimental SOFs. More specifically, it should correspond to the temperature below which the calculated SOFs start to deviate from the experimental data. This yields an estimate for the temperature, at which chemical order is frozen, between of 600 to 700 K.

Off-center displacements of Ba atoms

Experimental measurements of the nuclear density have shown a non-spherical distribution of the Ba atoms around the 6*d* sites of the type-I clathrate structure in several of the materials considered here.[3,11,13,14,40] This effect has also been included in Rietveld refinements of diffraction data by assigning six of the Ba atoms in the structure to either 24*k* or 24*j* Wyckoff sites with a partial occupancy of 25%, corresponding to a fourfold splitting of the 6*d* site. To assess whether this behavior can at least be partially explained in terms of the variation of chemical composition of the cages with Al/Ga content, we extracted representative configurations from MC simulations at 700 K and relaxed them using DFT calculations. We then mapped each configuration onto the respective ideal crystal structure scaled to the lattice parameter corresponding to the composition (Fig. S2 in the Supplementary Information), and computed the displacement of the Ba atom from the ideal 6*d* site.

In all four materials near the stoichiometric composition, the Ba atom is displaced by 15 to 19 pm from the ideal 6*d* site (Fig. 9). These numbers are in good agreement with

the radius of the ring-like nuclear density extracted experimentally.[3,13] Unfortunately, our statistics are insufficient in order to extract the full three-dimensional nuclear density. We can, however, obtain the radial distribution, which exhibits a shape that is consistent with a ring-like nuclear density [shown exemplarily for $Ba_8Al_xGe_{46-x}$ in Fig. 9(e)].

While in all four materials the off-center displacement (OCD) is maximal for $x \approx 16$, they exhibit differences with respect to its variation with composition. For $Ba_8Ga_xGe_{46-x}$ and $Ba_8Al_xGe_{46-x}$ the OCD falls off only slowly with Ga/Al content for $8 \leq x \leq 15$ with an average value of about 10 to 13 pm. In contrast, for the Si-containing clathrates the OCD decreases strongly and monotonically with composition, reaching minimal values of about 2 pm at $x \approx 6$.

The trends in the OCDs correlate with the variation of the lattice parameter with composition (Fig. S2 in the Supplementary Information). While in the case of $Ba_8Ga_xSi_{46-x}$ and $Ba_8Al_xSi_{46-x}$ the lattice parameter increases with Al/Ga content, a weaker correlation with the opposite sign is observed for $Ba_8Ga_xGe_{46-x}$ and $Ba_8Al_xGe_{46-x}$. The size of the cages, in which Ba resides, scales with the average atomic volume of the structure and thus the lattice constant (Fig. S5 in the Supplementary Information). The strong reduction in the OCD in the former two materials can therefore be related to a general decrease in the cage size.

It is noteworthy that the OCDs calculated here in the zero temperature limit, compare well both in trend and magnitude with experimental data for the atomic displacement parameter (ADP) of the Ba 6*d* site in $Ba_8Ga_xGe_{46-x}$ and $Ba_8Al_xSi_{46-x}$.[14,24] Since the ADPs indicate the magnitude of *thermal* displacements as obtained from Rietveld refinements, a direct comparison with the OCDs is, however, not meaningful. Nonetheless the underlying structural features including cage size and Al content of the cages are the same, which helps to explain the correlation of the parameters.

Comment on nuclear densities in $Ba_8Al_xGe_{46-x}$

The symmetry of the Ba site in $Ba_8Al_xGe_{46-x}$ appears to be sensitive to the synthesis route.[13] While for a "shake-and-bake" sample the Ba $6d$ site has been found to split four-fold at low temperatures yielding $24k$ or $24j$ sites, the $6d$ site symmetry was maintained in the case of a Czochralski grown crystal. This difference between the samples is also apparent from the nuclear densities. It has furthermore been found that the "shake and bake" sample had an Al content of 15.5 and a $6c$ SOF of 67%, whereas the Czochralski grown crystals gave 14.8 and 96%, respectively.[3] These two points fall in the composition region, for which our simulations show a relatively sharp transition in the SOFs (Fig. 7). The analysis of the Ba displacements shows that this transition also leads to a rather abrupt change in the OCDs, in accordance with the experimental trend.

Conclusions

In the present work, we have combined density functional theory calculations with alloy cluster expansions in order to study chemical ordering in four prototypical clathrates ($Ba_8Ga_xGe_{46-x}$, $Ba_8Ga_xSi_{46-x}$, $Ba_8Al_xGe_{46-x}$, $Ba_8Al_xSi_{46-x}$). The energy landscape was sampled as a function of temperature and composition using Monte Carlo simulations, from which we extracted site occupancy factors, heat capacities, and lattice constants.

The predicted SOFs are in very good agreement with experimental data, where comparison is possible (Fig. 7). More importantly the simulations clarify the experimental observations and reveal trends across materials. For Ga-based materials as well as Al-based materials with an Al content above $x = 14$, the different sites are occupied in the sequence $6c - 24k - 16i$. If the Al content drops, however, to $x \approx 14$ or below $16i$ sites become more preferable than $24k$ sites. This behavior can be explained in terms of the ECI parameters of the underlying CEs. The latter show that Al–Al repulsion is much stronger than Ga–Ga repulsion (Fig. 3), which drives the redistribution from $24k$ to $16i$ sites with decreasing Al

content.

Chemical ordering is shown to impact various properties including the heat capacity [Fig. 5(a) and Fig. S3 of the Supplementary Information] and the lattice parameter [Fig. 5(b,c) and Fig. S2 of the Supplementary Information]. Specifically, in the former case the present results suggest that the jump in the heat capacity observed in some experimental measurements can be related to the entropic contribution associated with chemical (dis)order.

For convenience let us summarize the essential chemical trends that have emerged from the comparison of four different clathrate systems. The singlet ECIs, which determine the energy cost for occupying different Wyckoff sites, follow the order $6c > 24k > 16i$ in all materials considered here. The pair interaction between group-13 species are, however, notably more repulsive for Al–Al than for Ga–Ga (Fig. 3). As a result, Al–Al bonds are strongly suppressed at all temperatures and compositions, whereas the Ga-based materials are more tolerant to the formation of Ga–Ga bonds (Fig. 6). The repulsive Al–Al interaction furthermore causes an inversion in the ordering of the SOFs for compositions above $x \approx 14$, with the $16i$ SOF exceeding the $24k$ SOF (Fig. 7). This behavior also translates to e.g., the heat capacity and the lattice parameter, for which the chemical ordering effect in Al-containing systems kicks in at higher temperatures than in Ga-based materials.

While the group-13 component is more dominant in the case of heat capacity, lattice parameter, and SOFs, the variation of lattice parameter and Ba OCD with composition is more sensitive to the group-14 component (Fig. 9 and Fig. S2 in the Supplementary Information). Here, both lattice constant and OCD in Si-based materials exhibit a pronounced positive correlation with Al/Ga-content. By contrast, a much weaker variation with the opposite sign is obtained for the lattice constant in the Ge-containing systems.

We note that in the present work we have made some approximations. Most notably although experimental data shows vacancies to be present in substantial concentrations, in particular at the lower end of the composition range, we did not include these defects in our simulations. As our results are in good or very good agreement with experimental data,

this reflects the fact that the inclusion of vacancies is of lesser importance for the properties considered here. Explicitly including vacancies implies moving from a quasi-binary (group-13/group-14) to a quasi-ternary (group-13/group-14/vacancy) system. While the inclusion of vacancies is beyond the scope of the present work, it can thus in principle be accomplished with cluster expansions and could be addressed in future work.

Generally, the present results demonstrate the potential of alloy cluster expansions to resolve microscopic features and reveal trends in complex inorganic materials that otherwise require extensive experimental work. This is not only very useful for understanding existing materials but ultimately creates an avenue for a more systematic exploration of a larger chemical space.

Supporting Information Available

Figures of 6*c* SOFs, lattice constants, and heat capacities as a function of temperature and composition; figures of effective cluster interactions for cluster expansions of the cell volume; compilation of experimental SOF data included in Fig. 7 in the form of a table (PDF); structures obtained by simulated annealing at different compositions (text files with atomic coordinates). This material is available free of charge via the Internet at `http://pubs.acs.org/`.

Acknowledgement

The authors gratefully acknowledge many helpful discussions with Joakim Brorsson and Anders Palmqvist. This work was funded by the Knut and Alice Wallenberg Foundation. Computer time allocations by the Swedish National Infrastructure for Computing at NSC (Linköping) and PDC (Stockholm) are gratefully acknowledged.

References

(1) Moss, G. P.; Smith, P. A. S.; Tavernier, D. Glossary of class names of organic compounds and reactivity intermediates based on structure (IUPAC Recommendations 1995). *Pure Appl. Chem.* **2009**, *67*, 1307–1375.

(2) Rogl, P. *Thermoelectrics Handbook*; CRC Press, 2005; Chapter 32, pp 1–24.

(3) Christensen, M.; Johnsen, S.; Iversen, B. B. Thermoelectric clathrates of type I. *Dalton Trans.* **2010**, *39*, 978–992.

(4) Toberer, E. S.; Christensen, M.; Iversen, B. B.; Snyder, G. J. High temperature thermoelectric efficiency in $Ba_8Ga_{16}Ge_{30}$. *Phys. Rev. B* **2008**, *77*, 075203.

(5) Nolas, G. S.; Cohn, J. L.; Slack, G. A.; Schujman, S. B. Semiconducting Ge clathrates: Promising candidates for thermoelectric applications. *Appl. Phys. Lett.* **1998**, *73*, 178–180.

(6) Christensen, S.; Schmkel, M. S.; Borup, K. A.; Madsen, G. K. H.; McIntyre, G. J.; Capelli, S. C.; Christensen, M.; Iversen, B. B. Glass-like thermal conductivity gradually induced in thermoelectric $Sr_8Ga_{16}Ge_{30}$ clathrate by off-centered guest atoms. *J. Appl. Phys.* **2016**, *119*, 185102.

(7) Shevelkov, A. V.; Kovnir, K. In *Zintl Phases*; Fässler, T. F., Ed.; Structure and Bonding 139; Springer Berlin Heidelberg, 2011; pp 97–142.

(8) Schäfer, H.; Eisenmann, B.; Müller, W. Zintl Phases: Transitions between Metallic and Ionic Bonding. *Angew. Chem., Int. Ed. Engl.* **1973**, *12*, 694–712.

(9) Eisenmann, B.; Schäfer, H.; Zagler, R. Die Verbindungen $A_8^{\mathrm{II}}B_{16}^{\mathrm{III}}B_{30}^{\mathrm{IV}}$ (A^{II} = Sr, Ba; B^{III}= Al, Ga; B^{IV} = Si, Ge, Sn) und ihre Käfigstrukturen. *J. Less-Common Met.* **1986**, *118*, 43–55.

(10) Shevelkov, A. V.; Kovnir, K. A.; Zaikina, J. V. *The Physics and Chemistry of Inorganic Clathrates*; Springer Series in Materials Science; Springer, Dordrecht, 2014; pp 125–167, DOI: 10.1007/978-94-017-9127-4_5.

(11) Christensen, M.; Lock, N.; Overgaard, J.; Iversen, B. B. Crystal Structures of Thermoelectric n- and p-type $Ba_8Ga_{16}Ge_{30}$ Studied by Single Crystal, Multitemperature, Neutron Diffraction, Conventional X-ray Diffraction and Resonant Synchrotron X-ray Diffraction. *J. Am. Chem. Soc.* **2006**, *128*, 15657–15665.

(12) Blake, N. P.; Bryan, D.; Latturner, S.; Møllnitz, L.; Stucky, G. D.; Metiu, H. Structure and stability of the clathrates $Ba_8Ga_{16}Ge_{30}$, $Sr_8Ga_{16}Ge_{30}$, $Ba_8Ga_{16}Si_{30}$, and $Ba_8In_{16}Sn_{30}$. *J. Chem. Phys.* **2001**, *114*, 10063–10074.

(13) Christensen, M.; Iversen, B. B. Host Structure Engineering in Thermoelectric Clathrates. *Chem. Mater.* **2007**, *19*, 4896.

(14) Roudebush, J. H.; de la Cruz, C.; Chakoumakos, B. C.; Kauzlarich, S. M. Neutron Diffraction Study of the Type I Clathrate $Ba_8Al_xSi_{46-x}$: Site Occupancies, Cage Volumes, and the Interaction between the Guest and the Host Framework. *Inorg. Chem.* **2012**, *51*, 1805–1812.

(15) Ångqvist, M.; Lindroth, D. O.; Erhart, P. Optimization of the Thermoelectric Power Factor: Coupling between Chemical Order and Transport Properties. *Chem. Mater.* **2016**, *28*, 6877–6885.

(16) Christensen, M.; Johnsen, S.; Söndergaard, M.; Overgaard, J.; Birkedal, H.; Iversen, B. B. Fast Preparation and Characterization of Quarternary Thermoelectric Clathrates. *Chem. Mater.* **2009**, *21*, 122–127.

(17) Troppenz, M.; Rigamonti, S.; Draxl, C. Predicting Ground-State Configurations and Electronic Properties of the Thermoelectric Clathrates $Ba_8Al_xSi_{46-x}$ and $Sr_8Al_xSi_{46-x}$. *Chem. Mater.* **2017**, *29*, 2414.

(18) Sanchez, J. M.; Ducastelle, F.; Gratias, D. Generalized cluster description of multicomponent systems. *Physica* **1984**, *128*, 334.

(19) Sanchez, J. M. Cluster expansion and the configurational theory of alloys. *Phys. Rev. B* **2010**, *81*, 224202.

(20) Candes, E.; Wakin, M. An Introduction To Compressive Sampling. *IEEE Signal Processing Magazine* **2008**, *25*, 21.

(21) Yin, W.; Osher, S.; Goldfarb, D.; Darbon, J. Bregman Iterative Algorithms for l_1-Minimization with Applications to Compressed Sensing. *SIAM Journal on Imaging Sciences* **2008**, *1*, 143–168.

(22) Goldstein, T.; Osher, S. The Split Bregman Method for L1-Regularized Problems. *SIAM Journal on Imaging Sciences* **2009**, *2*, 323–343.

(23) Nelson, L. J.; Hart, G. L. W.; Zhou, F.; Ozolins, V. Compressive sensing as a new paradigm for model building. *Phys. Rev. B* **2013**, *87*, 035125.

(24) Okamoto, N. L.; Kishida, K.; Tanaka, K.; Inui, H. Crystal structure and thermoelectric properties of type-I clathrate compounds in the Ba-Ga-Ge system. *J. Appl. Phys.* **2006**, *100*, 073504.

(25) We note that we have previously shown[15] that a unit cell is sufficient to obtain the SOFs with good accuracy.

(26) Sadigh, B.; Erhart, P. Calculations of excess free energies of precipitates via direct thermodynamic integration across phase boundaries. *Phys. Rev. B* **2012**, *86*, 134204.

(27) Blöchl, P. E. Projector augmented-wave method. *Phys. Rev. B* **1994**, *50*, 17953.

(28) Kresse, G.; Joubert, D. From ultrasoft pseudopotentials to the projector augmented-wave method. *Phys. Rev. B* **1999**, *59*, 1758.

(29) Kresse, G.; Furthmüller, J. Efficient iterative schemes for ab initio total-energy calculations using a plane-wave basis set. *Phys. Rev. B* **1996**, *54*, 11169.

(30) Kresse, G.; Furthmüller, J. Efficiency of ab-initio total energy calculations for metals and semiconductors using a plane-wave basis set. *Comp. Mater. Sci.* **1996**, *6*, 15–50.

(31) Perdew, J. P.; Burke, K.; Ernzerhof, M. Generalized Gradient Approximation Made Simple. *Phys. Rev. Lett.* **1996**, *77*, 3865–3868, erratum, *ibid.* **78**, 1396(E) (1997).

(32) Nelson, L. J.; Ozoliņš, V.; Reese, C. S.; Zhou, F.; Hart, G. L. W. Cluster expansion made easy with Bayesian compressive sensing. *Phys. Rev. B* **2013**, *88*, 155105.

(33) Togo, A.; Oba, F.; Tanaka, I. First-principles calculations of the ferroelastic transition between rutile-type and $CaCl_2$-type SiO_2 at high pressures. *Phys. Rev. B* **2008**, *78*, 134106.

(34) May, A. F.; Toberer, E. S.; Saramat, A.; Snyder, G. J. Characterization and analysis of thermoelectric transport in *n*-type $Ba_8Ga_{16-x}Ge_{30+x}$. *Phys. Rev. B* **2009**, *80*, 125205.

(35) Reardon, H.; Blichfeld, A. B.; Kasai, H.; Yin, H.; Bojesen, E. D.; Iversen, B. B. Revealing the slow decomposition kinetics of type-I clathrate $Ba_8Ga_{16}Ge_{30}$. *Phys. Chem. Chem. Phys.* **2017**, *19*, 15734.

(36) Nataraj, D.; Nagao, J. Structure and Raman scattering study on $Ba_8Ga_xSi_{46x}$ ($x = 10$ and 16) type I clathrates. *J. Solid State Chem.* **2004**, *177*, 1905 – 1911.

(37) Bentien, A.; Iversen, B.; Bryan, J.; Stucky, G.; Palmqvist, A.; Schultz, A.; Henning, R. Maximum entropy method analysis of thermal motion and disorder in thermoelectric clathrate $Ba_8Ga_{16}Si_{30}$. *J. Appl. Phys.* **2002**, *91*, 5694–5699.

(38) Bentien, A.; Nishibori, E.; Paschen, S.; Iversen, B. Crystal structures, atomic vibration, and disorder of the type-I thermoelectric clathrates $Ba_8Ga_{16}Si_{30}$, $Ba_8Ga_{16}Ge_{30}$, $Ba_8In_{16}Ge_{30}$, and $Sr_8Ga_{16}Ge_{30}$. *Phys. Rev. B* **2005**, *71*, 144107.

(39) Christensen, M.; Iversen, B. Investigations of Clathrate Type I Structures: $Ba_8Ga_{16}Si_{30}$. 2006; Proceedings of the 4th European Conference on Thermoelectrics edited by D. M. Rowe, Cardiff.

(40) Bobnar, M.; Böhme, B.; Wedel, M.; Burkhardt, U.; Ormeci, A.; Prots, Y.; Drathen, C.; Liang, Y.; Nguyen, H. D.; Baitinger, M.; Grin, Y. Distribution of Al atoms in the clathrate-I phase $Ba_8Al_xSi_{46-x}$ at $x = 6.9$. *Dalton Trans.* **2015**, *44*, 12680–12687.

(41) Erhart, P.; Albe, K. Thermodynamics of mono- and di-vacancies in barium titanate. *J. Appl. Phys.* **2007**, *102*, 084111.

Graphical TOC Entry

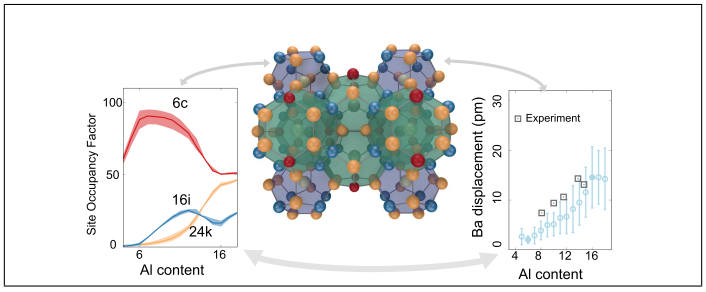

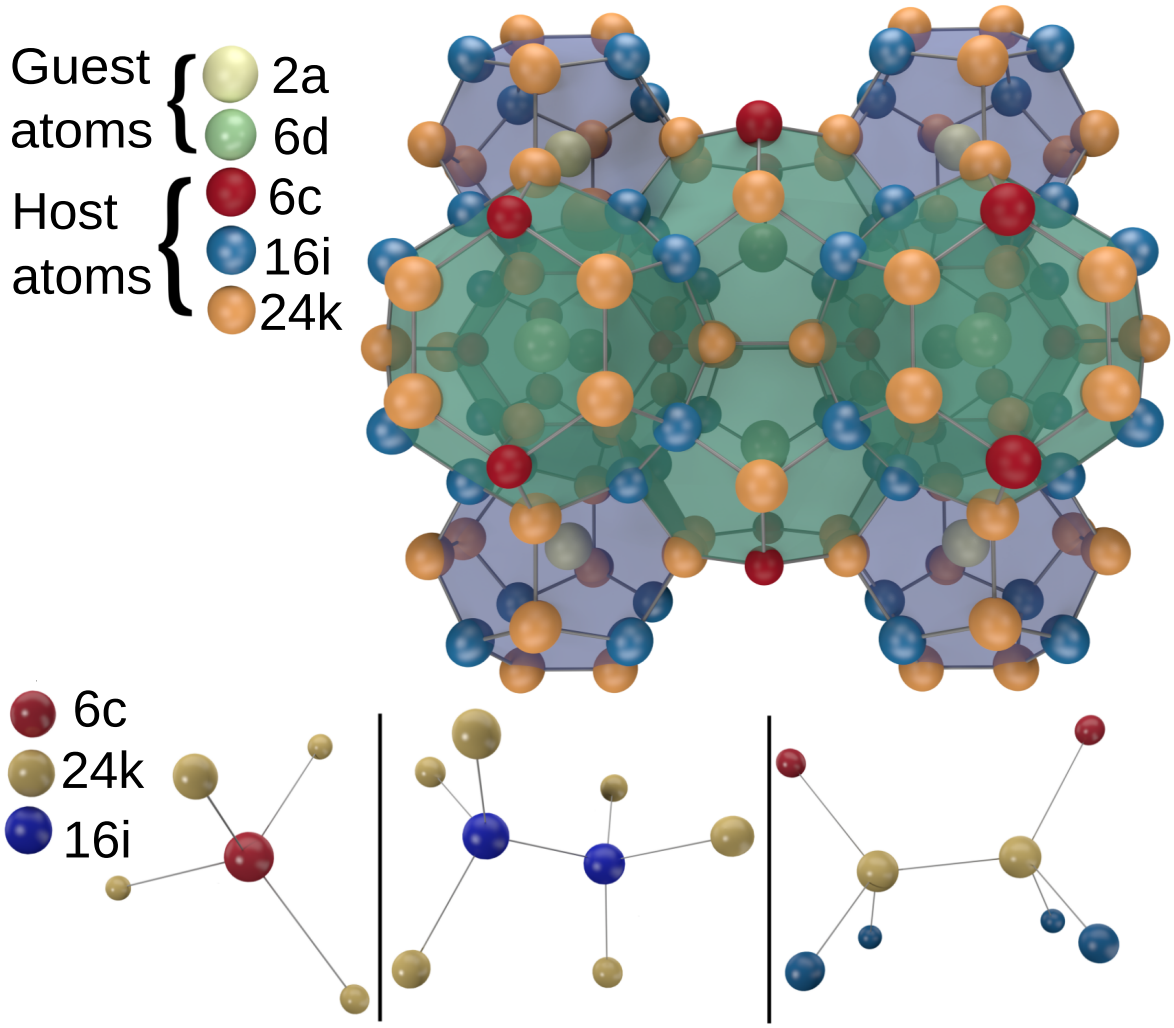

Figure 1: Crystal structure of type I clathrates. The guest species (Ba) occupies Wyckoff sites of type $2a$ and $6d$, while the host species (Ga, Al, Ge, Si) occupy Wyckoff sites of type $6c$, $16i$, and $24k$. The configurations in the bottom row illustrate the environments for $6c$, $16i$, and $24k$ sites, respectively.

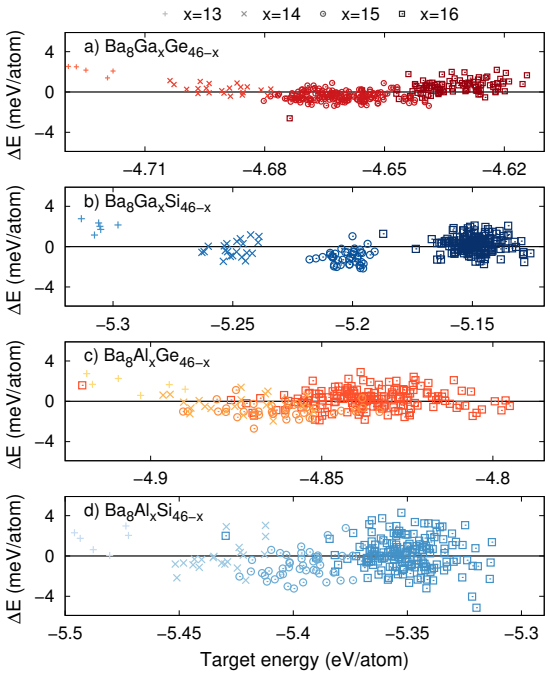

Figure 2: Performance of cluster expansions constructed in this work. Prediction errors for (a) $Ba_8Ga_xGe_{46-x}$, (b) $Ba_8Ga_xSi_{46-x}$, (c) $Ba_8Al_xGe_{46-x}$, and (d) $Ba_8Al_xSi_{46-x}$ as a function of the DFT target energy.

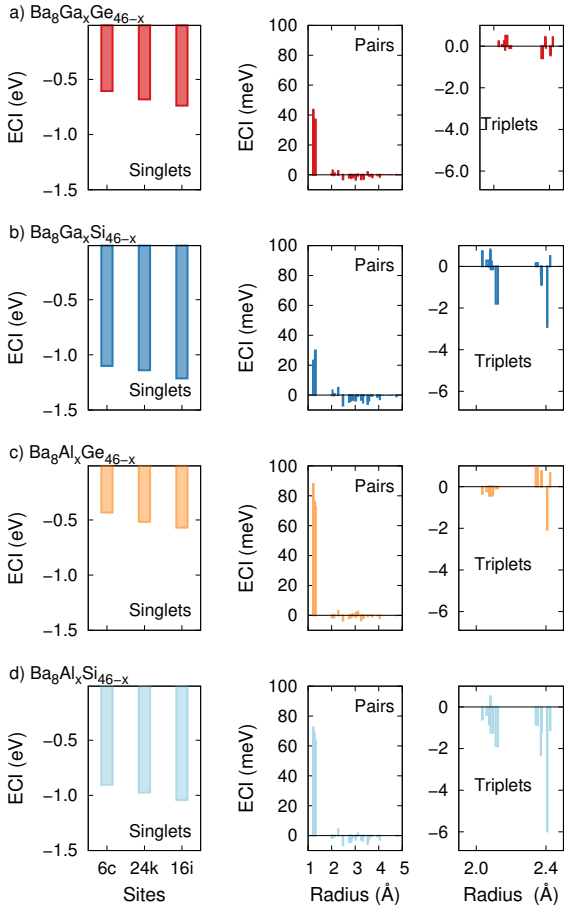

Figure 3: Effective cluster interactions as a function of cluster radius for (a) $Ba_8Ga_xGe_{46-x}$, (b) $Ba_8Ga_xSi_{46-x}$, (c) $Ba_8Al_xGe_{46-x}$, and (d) $Ba_8Al_xSi_{46-x}$ as a function of the radius.

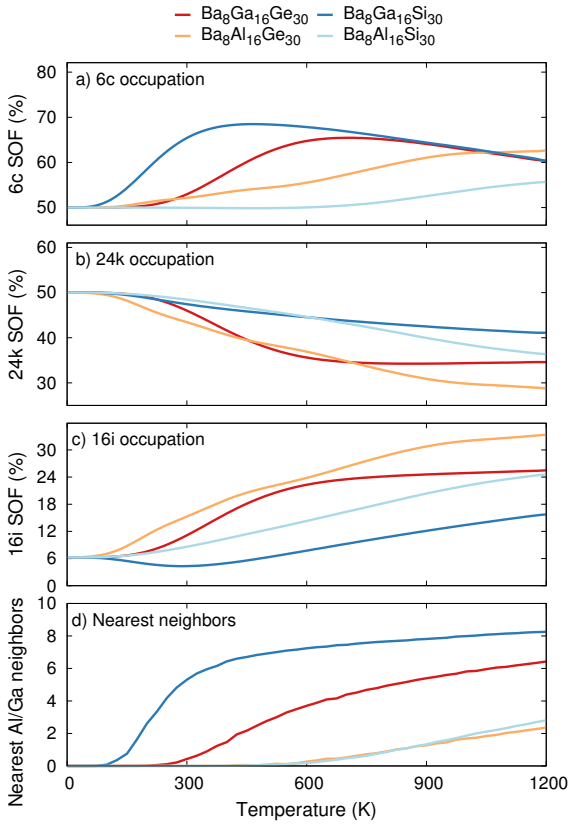

Figure 4: Site occupancy factors of stoichiometric intermetallic clathrates as a function of temperature for Wyckoff sites (a) 6*c*, (b) 24*k*, and (c) 16*i*. (d) Fraction of Al–Al or Ga–Ga nearest neighbors.

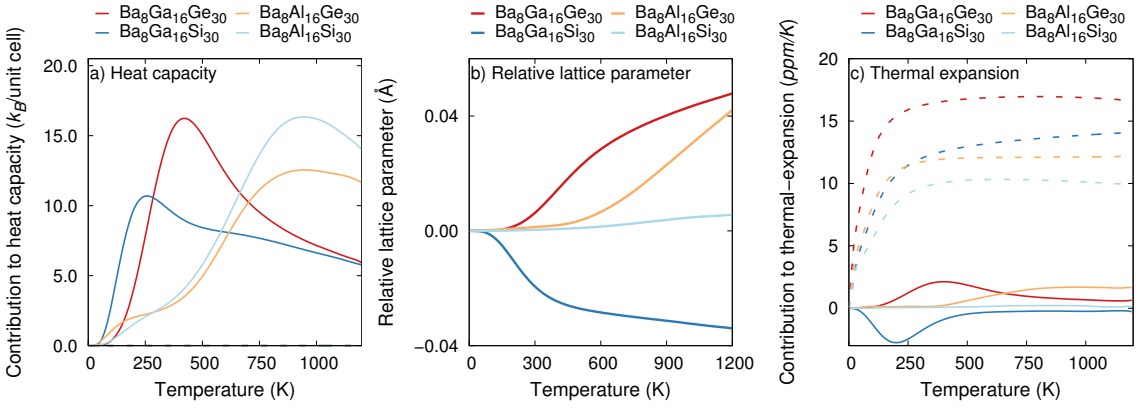

Figure 5: Contributions due to chemical ordering to (a) heat capacity and (b) lattice parameter. (c) Contribution to thermal expansion due to lattice vibrations (dotted lines) and chemical ordering (solid lines).

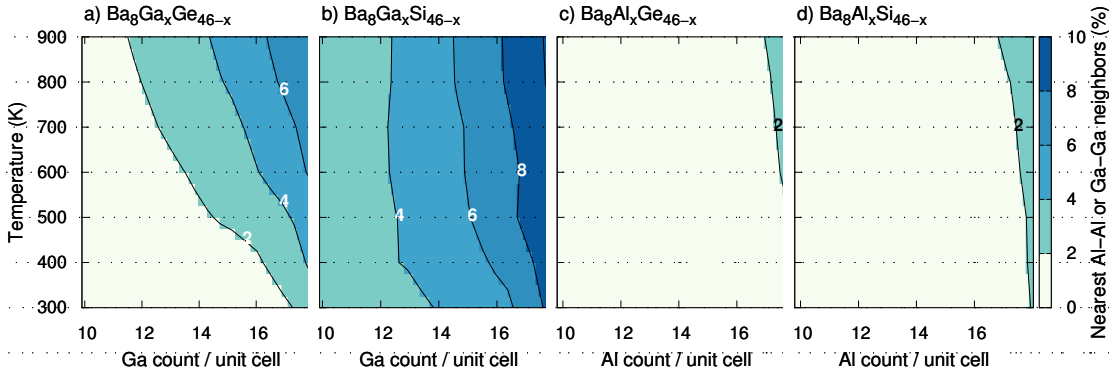

Figure 6: Fraction of Al–Al or Ga–Ga nearest neighbors for (a) $Ba_8Ga_xGe_{46-x}$, (b) $Ba_8Ga_xSi_{46-x}$, (c) $Ba_8Al_xGe_{46-x}$, and (d) $Ba_8Al_xSi_{46-x}$.

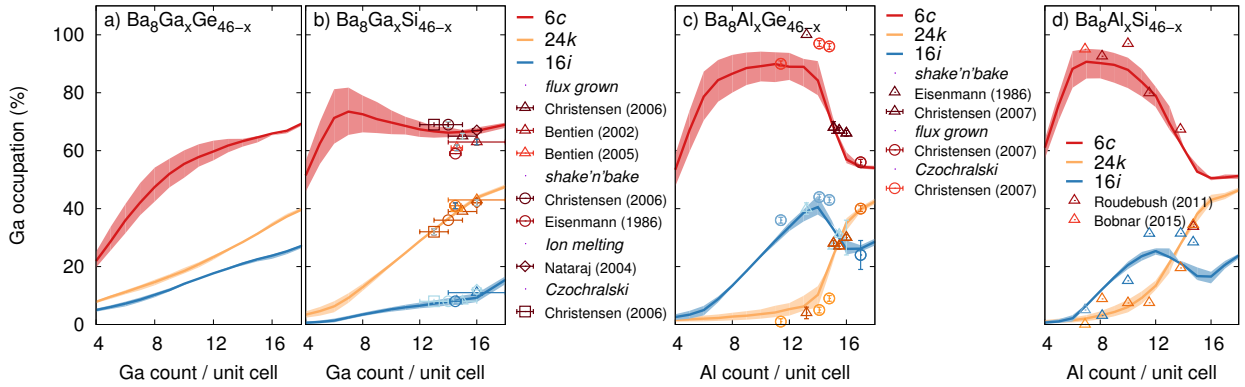

Figure 7: Site occupancy factors in intermetallic clathrates as a function of composition for Wyckoff sites 6*c* (red), 16*i* (blue), and 24*k* (orange). Solid lines show simulation results obtained at 700 K whereas the shaded regions indicate a variation by ± 100 K.

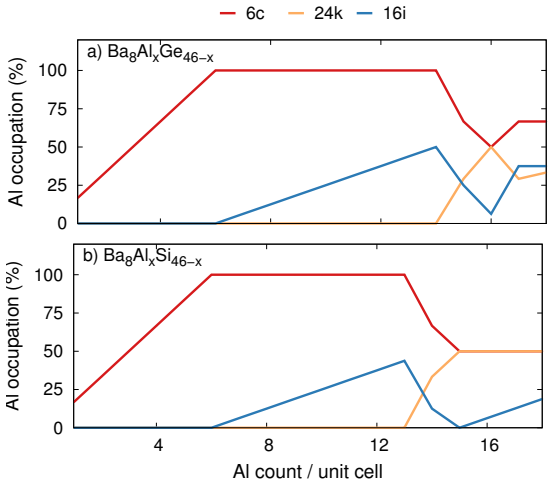

Figure 8: Site occupancy factors for the ground states in (a) $Ba_8Al_xSi_{46-x}$ and (b) $Ba_8Al_xGe_{46-x}$ as a function of composition for Wyckoff sites 6*c* (red), 16*i* (blue), and 24*k* (orange).

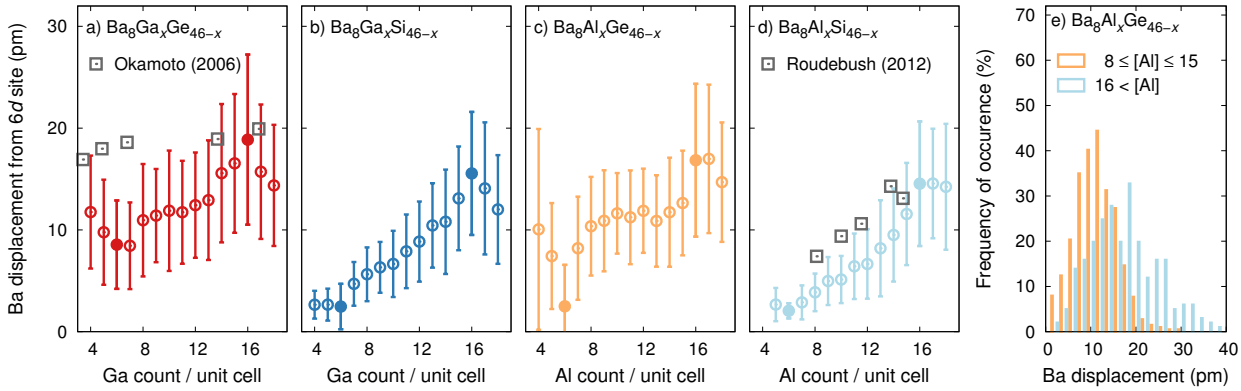

Figure 9: Off-center displacements of Ba atoms on 6*d* sites as a function of composition for (a) $Ba_8Ga_xGe_{46-x}$, (b) $Ba_8Ga_xSi_{46-x}$, (c) $Ba_8Al_xGe_{46-x}$, and (d) $Ba_8Al_xSi_{46-x}$ as well as the distribution of displacements for e) $Ba_8Al_xGe_{46-x}$. Experimental data for the atomic displacement parameters in $Ba_8Ga_xGe_{46-x}$ and $Ba_8Al_xSi_{46-x}$ have been taken from Refs. 24 and 14, respectively.